www.czasopisma.pan.pl PAN www.journals.pan.pl

INTL JOURNAL OF ELECTRONICS AND TELECOMMUNICATIONS, 2022, VOL. 68, NO. 3, PP. 527-533
Manuscript received March 29, 2022; revised August, 2022. DOI: 10.24425/ijet.2022.141270

Precision Calculations of the Characteristic Impedance of Complex Coaxial Waveguides Used in Wideband Thermal Converters of AC Voltage and Current

Krzysztof Kubiczek, and Marian Kampik

***Abstract*—The article presents precision and numerically stable method of calculation of the characteristic impedance of cylindrical multilayer waveguides used in high-precision wideband measuring instruments and standards, especially calculable thermal converters of AC voltage and precision wideband current shunts. Most of currently existing algorithms of characteristic impedance calculation of such waveguides are based upon approximations. Unfortunately, application of such methods is limited to waveguides composed of a specific, usually low number of layers. The accuracy of approximation methods as well as the number of layers is sometimes not sufficient, especially when the coaxial waveguide is a part of precision measurement equipment. The article presents the numerically stable matrix analytical formula using exponentially scaled modified Bessel functions to compute characteristic impedance and its components of the cylindrical coaxial multilayer waveguides. Results obtained with the developed method were compared with results of simulations made using the Finite Element Method (FEM) software simulations. Very good agreement between results of those two methods were achieved.**

***Keywords*—AC voltage standard; current shunt; characteristic impedance; multilayer cylindrical conductor; FEM simulation; modified Bessel functions; numerical stability; calorimetric thermal voltage converter; ac-dc transfer difference**

I. Introduction

Multilayer cylindrical waveguides are used in high-precision wideband measuring instruments and standards, including calculable thermal converters used in voltage AC-DC transfer [1],
[2] and precision high frequency current shunts [3]-[5]. Characteristic impedance of waveguides used in abovementioned metrology instruments must be calculated with a very high accuracy, achieving parts per million. One of the oldest concept of the waveguide is a cylindrical coaxial cable (coax) invented in 1880s and widely used presently [6], [7]. The development of the material science and techniques, such as electroless deposition of the metal onto the plastics (e.g. Teflon), opened up the new viabilities of the coaxial waveguides applications [8]. Due to the multilayer composition, the performance of the waveguide can be improved. Some of the stacked layers are used because of their good mechanical properties such as stiffness, while the others ensure high electrical conductivity, protection against oxidation, humidity or other environmental factors.

Today, one of the most popular approach of determination of the electrical parameters of cylindrical multilayer waveguides is the Finite Element Method [9]-[13]. The method allows computation of the characteristic impedance of the multilayer cylindrical conductors without usage of complex equations. However, usually it is necessary to use more than one solver, especially when the waveguide is working in wide frequency range [14]. The skin effect, which impact becomes substantial at higher frequencies, demands special meshing tools to ensure high level of accuracy.

On the other hand, the analytical methods of the computation of the characteristic impedance and its components can be implemented into the numerical software such as Mathematica, Matlab or its free equivalent software Octave. The analytical methods allow much faster computations than FEM. Moreover, characteristic impedance computation by analytical formulas allows easy implementation of the built-in algorithms, such as genetic ones, to provide the structure optimization.

Frankly speaking, in this sort of methods, magnetic vector potential is obtained from the product of the second order Maxwell's differential equations [15]. These solutions include the couples of the Bessel or similar functions [16]. Numerical calculations using these functions are often instable, especially for to low and high frequency, conductivity etc., respectively [17]. The calculation of wave impedance of the coax waveguide demands the knowledge of internal complex impedance of the inner and outer wire. Today, in the literature a few stable algorithms for computations of the impedance of the cylindrical structure, can be found. These methods use approximations, for example polynomial approximations [18], asymptotic approximation of equations of characteristic impedance [17], [19] approximation of the skin effect [20], [20], approximation of concentrated parameters by Gauss-Seidel algorithm [21]. The other group of numerically stable calculation formulas use scaled modified Bessel functions [22], [23].

Dr. Krzysztof Kubiczek is supported by the Foundation for Polish Science (FNP).

Authors are with Dept. of Measurement Science, Electronics and Control, Silesian University of Technology, Gliwice, Poland (e-mail: krzysztof.kubiczek@polsl.pl).

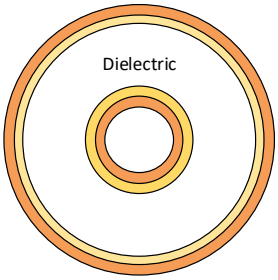

Fig. 1. The example of cross section of multi-layer cylindrical conductor

All of abovementioned methods are stable at extreme frequencies, but their results depend on the number of iterations or are suitable for coaxial waveguides composed of very limited structure only.

One of the method utilizing complex composition is presented in [24], but it does not consider the instability issue. Another approach described in [25] is a transfer matrix method of the multilayer composition. The stability have been provided by replacing Bessel functions with Hankel one for large arguments. However, the method is instable at very high frequencies [25]. The only known numerically stable method of computation of the internal impedance of the multilayer cable is the method described in [26]. The method is a combination of the transfer matrix and scaled modified Bessel functions method. It allows the computation of the internal impedance of the inner wire and its components also at high frequencies. Moreover, the method uses so called "fictional" layers to improve the computations in the case of the thick conducting layers. Actually, to the best of authors' knowledge, there is no known stable analytical formula of computations of the internal impedance of the outer wire of the coax with any number of layers.

In this article, we are going to propose numerically stable formulas for computations of the multilayer outer conductor parameters of the coaxial cable based on matrix approach, without number of layers restriction. Consequently, the methods presented in this article and in [26] allow computing together the characteristic impedance of the cylindrical waveguide for any number of layers with high accuracy and numerical stability. The proposed algorithm have been validated by comparing its results with results from simulations using FEM Ansys Multiphysics software [27]. The algorithm can be used in many different applications which call for high precision such as e.g. waveguides used in high frequency voltage or current standards.

II. The Impedance of the Multilayer Waveguide

A. Internal impedance of the multilayer inner wire

The cross section of assumed structure of the multi-layer circular waveguide is presented in Fig. 1. It is composed of two cylindrical conductors (centermost and outer), both built from more than one material. A dielectric (e.g. dry air) is located between both pipes. As a general rule, the characteristic impedance of the coaxial line per unit length (Z_c) is given by equation [28]:

$$Z_c = \sqrt{\frac{R + j\omega L}{G + j\omega C}}\,, \tag{1}$$

where ω is angular frequency, R, L, C, G are the resistance of the wires, inductance (internal and mutual), capacitance between wires and conductance of the dielectric between cylindrical conductors, respectively. The numerator of the equation (1) can be computed as the sum of internal impedance of the inner ($\bar{Z}_i$) and outer ($\bar{Z}_o$) pipes and mutual inductance between conductors as [29]:

$$Z_c = \sqrt{\frac{\bar{Z}_i + \bar{Z}_o + j\omega L_s}{G + j\omega C}}\,, \tag{2}$$

where L_s is a self-inductance per unit length determined by the outer dielectric diameter D and inner dielectric diameter d, given by:

$$L_s = \frac{\mu_0}{2\pi}\mu_r \ln\left(\frac{D}{d}\right). \tag{3}$$

The impedance of the dielectric between both cylindrical conductors is given by the capacitance and conductance:

$$C = \frac{2\pi\varepsilon'\varepsilon_0}{\ln\left(\frac{D}{d}\right)} \tag{4}$$

and

$$G = \frac{2\pi\omega\varepsilon_0\varepsilon''}{\ln\left(\frac{D}{d}\right)}, \tag{5}$$

where ε' and ε'' is the real and imaginary part of electric permittivity, respectively.

The complex impedance $\bar{Z}_i$ of the multilayer conductor is calculated by the matrix method described in [26]. The method allows the numerically stable computation of the $\bar{Z}_i$, even at high frequency and for thick layers as well.

B. Internal impedance of the thin multilayer outer wire

The cross section of the outer wire of a multilayer cylindrical waveguide is presented in Fig. 2.

It consists of N layers, where upper and lower boundaries, of a particular layer, are represented by r_{i+1} and r_i, respectively. The innermost layer is always assumed to be a perfect insulation (vacuum) of zero conductivity.

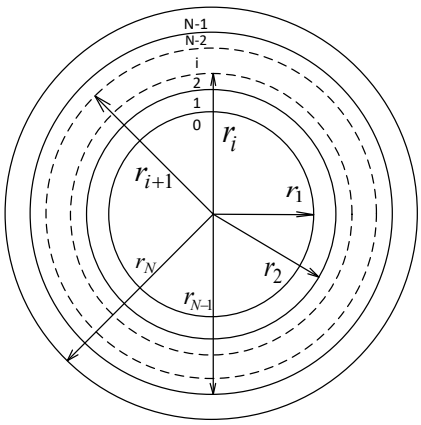

Fig. 2. The cross section of outer multilayer wire with particular boundaries

Physical properties of each *i*-th sections are: magnetic permeability μ_i and electrical conductivity σ_i. Each section has also its wave number $\bar{\gamma}_i$ [30]:

$$\bar{\gamma}_i = \sqrt{\mathrm{j}\sigma_i\mu_i\omega - \omega^2\varepsilon_i\mu_i}\ . \tag{6}$$

Following the Poynting's theorem of conservation of energy [31], the internal impedance of the outer wire is given by:

$$\bar{Z}_o = \frac{1}{2\pi r_1}\cdot\frac{\bar{E}_1\big|_{r=r_1}}{\bar{H}_1\big|_{r=r_1}}\ , \tag{7}$$

where $\bar{E}_1$ and $\bar{H}_1$ are the phasors of electrical field intensity and magnetic field intensity in the first layer, respectively. Because the current of the outer pipe flows in opposite direction to the current in the inner wire, the boundary conditions for the electric and magnetic field intensities of particular layers can be expressed as:

$$\begin{cases} \bar{H}_i\big|_{r=r_i} = \bar{H}_{i+1}\big|_{r=r_i} \\ \bar{E}_i\big|_{r=r_i} = \bar{E}_{i+1}\big|_{r=r_i} \\ \bar{H}_1\big|_{r=r_1} = \dfrac{-\bar{I}}{2\pi r_1} \end{cases}\ , \tag{8}$$

where $\bar{I}$ represents the phasor of the total current flowing in a wire or pipe. The upper boundary of the outermost layer N ($r = r_N$) has a boundary condition:

$$\bar{H}_N\big|_{r=r_N} = 0\ . \tag{9}$$

Assuming longitudinal current and neglecting proximity effect due to perfect concentricity of the geometry of the inner wire and outer pipe, using the cylindrical coordinate system, the phasor of magnetic field intensity, given by second order Maxwell's differential equation is in the form [32]:

$$r^2\frac{\partial^2\bar{H}_i}{\partial r^2} + r\frac{\partial\bar{H}_i}{\partial r} - \left(\bar{\gamma}_i^{\,2}\cdot r^2 + 1\right)\bar{H}_i = 0\ . \tag{10}$$

The solution of equation (10) as well as Ampere's law, phasors of the electric and magnetic field intensities in the *i*-th layer, presented in [30], have the form:

$$\begin{cases} \bar{H}_i = \bar{C}_i\cdot\bar{I}_1(\bar{\gamma}_i\cdot r_i) + \bar{D}_i\cdot\bar{K}_1(\bar{\gamma}_i\cdot r_i) \\ \bar{E}_i = \dfrac{\bar{\gamma}_i}{\sigma_i}\left[\bar{C}_i\cdot\bar{I}_0(\bar{\gamma}_i\cdot r_i) - \bar{D}_i\cdot\bar{K}_0(\bar{\gamma}_i\cdot r_i)\right] \end{cases} \tag{11}$$

where $\bar{C}_i$, $\bar{D}_i$ are the unknown complex-valued coefficients for the *i*-th layer, $\bar{I}_1$, $\bar{K}_1$, $\bar{I}_0$ and $\bar{K}_0$ are the complex-valued modified Bessel functions of the first kind of order one, second kind of order one, first kind of order zero and the second kind of order zero, respectively.

The phasors of the electric and magnetic fields intensities of the i+1 layer, using the boundary conditions (8), have the form:

$$\begin{cases} \bar{H}_{i+1} = \bar{C}_i\cdot\bar{I}_1(\bar{\gamma}_i\cdot r_{i+1}) + \bar{D}_i\cdot\bar{K}_1(\bar{\gamma}_i\cdot r_{i+1}) \\ \bar{E}_{i+1} = \dfrac{\bar{\gamma}_i}{\sigma_i}\left[\bar{C}_i\cdot\bar{I}_0(\bar{\gamma}_i\cdot r_{i+1}) - \bar{D}_i\cdot\bar{K}_0(\bar{\gamma}_i\cdot r_{i+1})\right] \end{cases}. \tag{12}$$

Parameters $\bar{C}_i$ and $\bar{D}_i$ are calculated after converting the equation (12) into the matrix form:

$$\begin{bmatrix}\bar{C}_i\\ \bar{D}_i\end{bmatrix} = \frac{1}{\Delta_i}\begin{bmatrix}\bar{K}_1(\bar{\gamma}_i\cdot r_{i+1}) & \bar{K}_0(\bar{\gamma}_i\cdot r_{i+1})\\ -\bar{I}_1(\bar{\gamma}_i\cdot r_{i+1}) & \bar{I}_0(\bar{\gamma}_i\cdot r_{i+1})\end{bmatrix}\begin{bmatrix}\sigma_i & 0\\ \bar{\gamma}_i & \\ 0 & 1\end{bmatrix}\begin{bmatrix}\bar{E}_{i+1}\\ \bar{H}_{i+1}\end{bmatrix}, \tag{13}$$

where Δ_i is a determinant equal to:

$$\Delta_i = \bar{I}_0(\bar{\gamma}_i\cdot r_{i+1})\cdot\bar{K}_1(\bar{\gamma}_i\cdot r_{i+1}) + \bar{I}_1(\bar{\gamma}_i\cdot r_{i+1})\cdot\bar{K}_0(\bar{\gamma}_i\cdot r_{i+1})\ . \tag{14}$$

Aiming the Wronskian of modified Bessel functions [33], the equation (14) can be substituted by its simplified form:

$$\Delta_i = \frac{1}{\bar{\gamma}_i\cdot r_{i+1}}\ . \tag{15}$$

Finally, substituting (13) into the equation (11), the dependence between electric and magnetic field phasors of upper and lower boundaries of the particular layer can be expressed as:

$$\begin{bmatrix}\bar{E}_i\\ \bar{H}_i\end{bmatrix} = \mathrm{T}_i\begin{bmatrix}\bar{E}_{i+1}\\ \bar{H}_{i+1}\end{bmatrix}, \tag{16}$$

where T_i is the transfer matrix equal to:

$$\mathrm{T}_i = \begin{bmatrix}a_i & b_i\\ c_i & d_i\end{bmatrix}. \tag{17}$$

The matrix T_i can be converted using equations (11) and (12) to the matrix form:

$$\begin{bmatrix}a_i & b_i\\ c_i & d_i\end{bmatrix} = \begin{bmatrix}\bar{\gamma}_i & 0\\ \sigma_i & \\ 0 & 1\end{bmatrix}\begin{bmatrix}\bar{I}_0(\bar{\gamma}_i\cdot r_i) & -\bar{K}_0(\bar{\gamma}_i\cdot r_i)\\ \bar{I}_1(\bar{\gamma}_i\cdot r_i) & \bar{K}_1(\bar{\gamma}_i\cdot r_i)\end{bmatrix} \times\begin{bmatrix}\bar{K}_1(\bar{\gamma}_i\cdot r_{i+1}) & \bar{K}_0(\bar{\gamma}_i\cdot r_{i+1})\\ -\bar{I}_1(\bar{\gamma}_i\cdot r_{i+1}) & \bar{I}_0(\bar{\gamma}_i\cdot r_{i+1})\end{bmatrix}\begin{bmatrix}\dfrac{\sigma_i}{\Delta_i\,\bar{\gamma}_i} & 0\\ 0 & \dfrac{1}{\Delta_i}\end{bmatrix}. \tag{18}$$

The results of (18) are:

$$a_i = \frac{1}{\Delta_i}\left[\bar{I}_0(\bar{\gamma}_i\cdot r_i)\cdot\bar{K}_1(\bar{\gamma}_i\cdot r_{i+1}) + \bar{K}_0(\bar{\gamma}_i\cdot r_i)\cdot\bar{I}_1(\bar{\gamma}_i\cdot r_{i+1})\right], \tag{19}$$

$$b_i = \frac{\bar{\gamma}_i}{\sigma_i\Delta_i}\left[\bar{I}_0(\bar{\gamma}_i\cdot r_i)\cdot\bar{K}_0(\bar{\gamma}_i\cdot r_{i+1}) - \bar{K}_0(\bar{\gamma}_i\cdot r_i)\cdot\bar{I}_0(\bar{\gamma}_i\cdot r_{i+1})\right], \tag{20}$$

$$c_i = \frac{\sigma_i}{\bar{\gamma}_i\Delta_i}\left[\bar{I}_1(\bar{\gamma}_i\cdot r_i)\cdot\bar{K}_1(\bar{\gamma}_i\cdot r_{i+1}) - \bar{K}_1(\bar{\gamma}_i\cdot r_i)\cdot\bar{I}_1(\bar{\gamma}_i\cdot r_{i+1})\right], \tag{21}$$

$$d_i = \frac{1}{\Delta_i}\left[\bar{I}_1(\bar{\gamma}_i\cdot r_i)\cdot\bar{K}_0(\bar{\gamma}_i\cdot r_{i+1}) + \bar{K}_1(\bar{\gamma}_i\cdot r_i)\cdot\bar{I}_0(\bar{\gamma}_i\cdot r_{i+1})\right]\ . \tag{22}$$

The internal impedance of the outermost region lower boundary is defined as:

$$\bar{Z}_{N-1} = \frac{\bar{E}_{N-1}}{\bar{H}_{N-1}} = \frac{a_{N-1}}{c_{N-1}} = \frac{\bar{\gamma}_{N-1}}{\sigma_{N-1}} \times\left[\frac{\bar{I}_0(x_N')\cdot\bar{K}_1(x_N) + \bar{K}_0(x_N')\cdot\bar{I}_1(x_N)}{\bar{I}_1(x_N')\cdot\bar{K}_1(x_N) - \bar{K}_1(x_N')\cdot\bar{I}_1(x_N)}\right], \tag{23}$$

where $x_N = \bar{\gamma}_{N-1}\cdot r_N$ and $x_N' = \bar{\gamma}_{N-1}\cdot r_{N-1}$.

The impedance of the first layer can be performed from transfer matrixes as:

$$\begin{bmatrix} \bar{E}_1 \\ \bar{H}_1 \end{bmatrix} = \mathrm{T} \begin{bmatrix} \bar{E}_{N-1} \\ \bar{H}_{N-1} \end{bmatrix}; \ \mathrm{T} = \prod_{i=1}^{N-1} T_i \tag{24}$$

and the impedance of the first layer is:

$$\bar{Z}_1 = \frac{a\bar{Z}_{N-1} + b}{c\bar{Z}_{N-1} + d}. \tag{25}$$

Using the equation (7) and boundary conditions, the impedance of the outermost wire is:

$$\bar{Z}_o = \frac{-\bar{Z}_1}{2\pi r_1}. \tag{26}$$

Resistance R and internal inductance L can be calculated as:

$$\begin{cases} R = \mathrm{Re}\{\bar{Z}_o\} \\ L = \dfrac{\mathrm{Im}\{\bar{Z}_o\}}{\omega} \end{cases}, \tag{27}$$

where $\mathrm{Re}\{\bar{Z}_o\}$ and $\mathrm{Im}\{\bar{Z}_o\}$ denote the real and imaginary part of $\bar{Z}_o$, respectively.

The numerical computations of modified Bessel functions in equations (19) – (23) are numerically unstable, especially at higher frequencies. To get rid of the instability, the modified Bessel functions are exchanged with scaled modified Bessel functions according to their definition [23]:

$$\bar{I}_n^s(x) = \exp(-x) \cdot \bar{I}_n \tag{28}$$

$$\bar{K}_n^s(x) = \exp(x) \cdot \bar{K}_n, \tag{29}$$

where $\bar{I}_n^s$ is a scaled modified Bessel function of the first kind of order n and $\bar{K}_n^s$ is a scaled modified Bessel function of the second kind of order n. The computation methods of the scaled modified Bessel functions with discussion are presented in [32].

Taking (28) and (29) into account, the equations (19) – (23) can be rewritten as:

$$\begin{aligned} a_i = \frac{1}{\Delta_i}\big[& \bar{I}_0^s(\bar{\gamma}_i \cdot r_i) \cdot \bar{K}_1^s(\bar{\gamma}_i \cdot r_{i+1}) \exp[\bar{\gamma}_i(r_i - r_{i+1})] \\ & + \bar{K}_0^s(\bar{\gamma}_i \cdot r_i) \cdot \bar{I}_1^s(\bar{\gamma}_i \cdot r_{i+1}) \exp[\bar{\gamma}_i(r_{i+1} - r_i)] \big] \end{aligned} \tag{30}$$

$$\begin{aligned} b_i = \frac{\bar{\gamma}_i}{\sigma_i \Delta_i}\big[& \bar{I}_0^s(\bar{\gamma}_i \cdot r_i) \cdot \bar{K}_0^s(\bar{\gamma}_i \cdot r_{i+1}) \exp[\bar{\gamma}_i(r_i - r_{i+1})] \\ & - \bar{K}_0^s(\bar{\gamma}_i \cdot r_i) \cdot \bar{I}_0^s(\bar{\gamma}_i \cdot r_{i+1}) \exp[\bar{\gamma}_i(r_{i+1} - r_i)] \big] \end{aligned} \tag{31}$$

$$\begin{aligned} c_i = \frac{\sigma_i}{\bar{\gamma}_i \Delta_i}\big[& \bar{I}_1^s(\bar{\gamma}_i \cdot r_i) \cdot \bar{K}_1^s(\bar{\gamma}_i \cdot r_{i+1}) \exp[\bar{\gamma}_i(r_i - r_{i+1})] \\ & - \bar{K}_1^s(\bar{\gamma}_i \cdot r_i) \cdot \bar{I}_1^s(\bar{\gamma}_i \cdot r_{i+1}) \exp[\bar{\gamma}_i(r_{i+1} - r_i)] \big] \end{aligned} \tag{32}$$

$$\begin{aligned} d_i = \frac{1}{\Delta_i}\big[& \bar{I}_1^s(\bar{\gamma}_i \cdot r_i) \cdot \bar{K}_0^s(\bar{\gamma}_i \cdot r_{i+1}) \exp[\bar{\gamma}_i(r_i - r_{i+1})] \\ & + \bar{K}_1^s(\bar{\gamma}_i \cdot r_i) \cdot \bar{I}_0^s(\bar{\gamma}_i \cdot r_{i+1}) \exp[\bar{\gamma}_i(r_{i+1} - r_i)] \big] \end{aligned} \tag{33}$$

and

$$\begin{aligned} \bar{Z}_{N-1} = \frac{\bar{\gamma}_{N-1}}{\sigma_{N-1}} \times \Bigg[& \frac{\bar{I}_0(x_N') \cdot \bar{K}_1(x_N) \exp[x_N' - x_N]}{\bar{I}_1(x_N') \cdot \bar{K}_1(x_N) \exp[x_N' - x_N]} \\ & \frac{+ \bar{K}_0(x_N') \cdot \bar{I}_1(x_N) \exp[x_N - x_N']}{- \bar{K}_1(x_N') \cdot \bar{I}_1(x_N) \exp[x_N - x_N']} \Bigg] \end{aligned} \tag{34}$$

$\bar{Z}_1$ and $\bar{Z}_o$ are computed using equations (25) and (26), respectively.

The numerically stable solution of the equations (30) - (34) is provided by reduction of the argument of the exponent equal to $\bar{\gamma}_i(r_i - r_{i+1})$ and $\bar{\gamma}_i(r_{i+1} - r_i)$. However, at higher frequencies and for thick layers, the computed parameters a_i, b_i, c_i, d_i and, as a consequence, $\bar{Z}_i$ are large and cause numerical instability. To reduce values of mentioned parameters, thick layers can be divided into additional thin "fictional" layers. This approach is described in [26] in details.

III. The Validation of the New Analitycal Formula

A. *Multi-thin-layer coaxial waveguide computation*

In the first exemplary calculation, the structure of the coaxial conductor presented in Fig. 3 was considered. This waveguide is composed of two cylindrical conductors. The core of internal cylindrical wire of radius equal to 0.7 mm is made of stainless steel of relative permeability 1.02 and electrical conductivity $1.32 \cdot 10^6$ S/m. The next layer is 10 μm thick copper of relative permeability 0.99994 and electrical conductivity $5.96 \cdot 10^7$ S/m. The last layer is 5 μm thick gold of relative permeability 0.999966 and electrical conductivity $4.4 \cdot 10^7$ S/m. The relative permittivity was set to 1 for all of used materials. The outer cylindrical conductor is composed of three conductive materials. The first layer (counting from the inside) is 5 μm thick gold, then 10 μm thick copper and then stainless steel pipe of 100 μm thick wall. The inner radius of gold layer is 1.6 mm. The insulation is dry air of relative permeability and permittivity equal to 1.00054 and 1, respectively. The conductivity of air was assumed as equal to 0. Exactly the same material properties, geometry and dimensions were implemented into the Matlab, to prepare calculations by the developed formulas and to ANSYS FEM software. The FEM solvers were chosen depending on frequency. For lower frequencies (conventionally when the $\lambda > 100D$), *Maxwell* solver was chosen, while for higher frequencies ($\lambda \leq 100D$), *High-Frequency Structure Simulator (HFSS).* The detailed description of methods and solvers used in validation may be found in [14].

As stated previously, the presented analytical formula allows to calculate the characteristic impedance of the Transverse Electro-Magnetic (TEM) mode. The cut-off frequency of the TE_{11}, calculated according to [34], equals approximately 41.5 GHz for the assumed geometry of the coax.

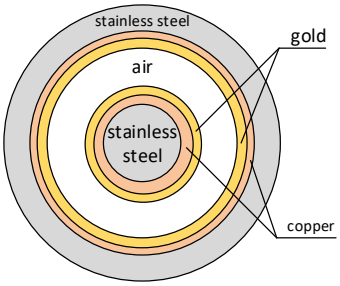

Fig. 3. The cross section of the multilayer coaxial waveguide, used in the first example

TABLE I
COMPARISON OF THE MODULE OF CHARACTERISTIC IMPEDANCE OF COAXIAL WAVEGUIDE FROM THE FIRST EXAMPLE

f	$\|Z\|$ Matlab	$\|Z\|$ ANSYS	$\Delta\|Z\|$ Matlab - ANSYS	$\Delta\|Z\|$
Hz	Ω	Ω	Ω	%
10^0	25424	25431	7	0.027
10^1	8039.9	8042.1	2.2	
10^2	2542.4	2543.1	0.7	
10^3	804.00	804.21	0.22	
10^4	254.34	254.41	0.07	
10^5	83.227	83.249	0.022	
10^6	50.382	50.395	0.014	
10^7	48.737	48.750	0.013	
10^8	48.534	48.541	0.006	0.013
10^9	48.368	48.383	0.015	0.031
10^{10}	48.318	48.333	0.015	0.031
$4{\cdot}10^{10}$	48.307	48.321	0.015	0.030

Therefore, the computations were performed in the frequency range from 1 Hz to 40 GHz. The TE_{11} and higher order modes are insignificant and their propagation is negligibly small. The module of characteristic impedance, resistance per unit length and inductance per unit length is presented in Tab. I, Tab II and Tab. III, respectively.

The difference between modules of characteristic impedance calculated with Matlab and FEM models, shown in Tab. I, is between 0.006 Ω and 7 Ω, i.e. the relative difference is from 0.013% to 0.027%, respectively. Calculated values of characteristic impedance module shown in Tab. I strongly confirm correctness of new analytical formulas presented in this paper. In the whole assumed frequency range, the relative difference between Matlab and ANSYS results is less than 0.04%.

Table II contains results of resistance calculations from the first example. The absolute difference between results obtained from our method and from FEM simulations equals zero in frequency range from 1 to 10^7 Hz. The difference increases above 100 MHz. The highest difference between results obtained with analytical model and FEM simulations is at 40 GHz, which is close to the waveguide cut-off frequency. The relative difference is equal to approximately 2%. Nevertheless, it is less than 0.15% in frequency range from 1 Hz to 10 GHz.

The last comparison of the parameters of the first structure, inductance per unit length, is presented in Table III.

TABLE II
COMPARISON OF RESISTANCE PER UNIT LENGTH OF COAXIAL WAVEGUIDE FROM THE FIRST EXAMPLE

f	R Matlab	R ANSYS	ΔR Matlab - ANSYS	ΔR
Hz	Ω/m	Ω/m	Ω/m	%
10^0	0.2806685	0.2806685	0	>0.01
10^1	0.2806685	0.2806685		
10^2	0.2806685	0.2806685		
10^3	0.2806685	0.2806685		
10^4	0.2806714	0.2806714		
10^5	0.2809538	0.2809538		
10^6	0.3003694	0.3003695		
10^7	0.3733909	0.3733909		
10^8	0.8968540	0.8968598	0.0000058	
10^9	3.0633201	3.0635665	0.0002464	0.01
10^{10}	9.6498060	9.6366049	0.0132012	0.14
$4{\cdot}10^{10}$	19.2967858	18.9145209	0.3822649	2.02

TABLE III
COMPARISON OF THE INDUCTANCE PER UNIT LENGTH OF COAXIAL WAVEGUIDE FROM THE FIRST EXAMPLE

f	L Matlab	L ANSYS	ΔL Matlab - ANSYS	L
Hz	μH/m	μH/m	μH/m	%
10^0	0.1708578	0.1708578	0	>0.01
10^1	0.1708578	0.1708578		
10^2	0.1708578	0.1708578		
10^3	0.1708578	0.1708578		
10^4	0.1708575	0.1708575		
10^5	0.1708273	0.1708273		
10^6	0.1687718	0.1687718		
10^7	0.1640388	0.1640388		
10^8	0.1627767	0.1627772	0.0000005	
10^9	0.1616674	0.1616791	0.0000117	
10^{10}	0.1613358	0.1613468	0.0000110	
$4{\cdot}10^{10}$	0.1612590	0.1612687	0.0000097	

Similarly to the case of the resistance, the nominal difference between inductance per unit length, calculated using the new developed Matlab formula and FEM software is equal to zero in the frequency range from 1 to 10^7 Hz. Above this frequency, the difference is slightly rising, but the relative difference remains below 0.01%, which strongly confirms correctness of the new analytical formula.The capacitance calculated using the Matlab formula and FEM simulation equals 69.11 and 69.07 pF/m, respectively. It corresponds to absolute difference equal to 0.04 pF/m, or 0.05% relatively.

B. Thick-layer coaxial waveguide computation

In the second example, a thick-wall coaxial waveguide will be considered. Its geometry is presented in Fig. 4. The inner cylindrical conductor of 2 mm radius is made from copper. The outer copper tubular conductor has the internal radius equal to 4.6 mm and external 6.6 mm, which corresponds to the 2 mm wall thickness. The space between both conductors is filled with dry air. The physical properties of air and copper are the same as in the first example. The thick walls of the outer conductor are the potential reason of numerical instability at high frequencies.

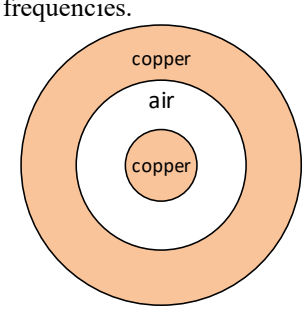

Fig. 4. The cross section of the coaxial waveguide, used in the second example.

Therefore calculations were performed using 1) Matlab without additional "fictional" layers, 2) Matlab with additional "fictional" layers as presented in [26] and 3) ANSYS FEM simulations. Numerical instability in the assumed range of frequency disappears when the number of fictional layers equals 8. The cut-off frequency for this geometry is approximately 14.5 GHz. Thus, the parameters were calculated in the frequency range from 1 Hz to 14 GHz. The calculated results: the module of characteristic impedance, resistance per unit length and inductance per unit length are presented in Tab. IV, V and VI, respectively.

TABLE IV
COMPARISON OF THE MODULE OF CHARACTERISTIC IMPEDANCE OF COAXIAL WAVEGUIDE FROM THE SECOND EXAMPLE

f	$\|Z\|$ Matlab without fictional layers	$\|Z\|$ Matlab with fictional layers	$\|Z\|$ ANSYS	$\Delta\|Z\|$ Matlab - ANSYS	$\Delta\|Z\|$
Hz	Ω	Ω	Ω	Ω	%
10^0	1936	1936	1937	1	0.06
10^1	612.2	612.2	612.6	0.4	0.06
10^2	194.08	194.08	194.20	0.12	0.06
10^3	72.888	72.888	72.931	0.042	0.06
10^4	57.232	57.232	57.264	0.032	0.06
10^5	52.197	52.197	52.226	0.029	0.06
10^6	50.645	50.645	50.674	0.028	0.06
10^7	50.162	50.162	50.190	0.028	0.06
10^8	50.010	50.010	50.024	0.014	0.03
10^9	NaN	49.962	49.976	0.014	0.03
10^{10}	NaN	49.947	49.961	0.014	0.03
$1.4\cdot10^{10}$	NaN	49.946	49.960	0.014	0.03

TABLE V
COMPARISON OF THE RESISTANCE PER UNIT LENGTH OF COAXIAL WAVEGUIDE FROM THE SECOND EXAMPLE

f	R Matlab without fictional layers	R Matlab with fictional layers	R ANSYS	ΔR Matlab - ANSYS	ΔR
Hz	Ω/m	Ω/m	Ω/m	Ω/m	%
10^0	0.0015736	0.0015736	0.0015742	0.0000006	0.04
10^1	0.0015736	0.0015736	0.0015742	0.0000006	0.04
10^2	0.0015741	0.0015741	0.0015746	0.0000006	0.04
10^3	0.0016194	0.0016194	0.0016199	0.0000006	0.03
10^4	0.0032419	0.0032419	0.0032426	0.0000006	0.02
10^5	0.0095770	0.0095770	0.0095789	0.0000018	0.02
10^6	0.0296605	0.0296605	0.0296650	0.0000045	0.02
10^7	0.0931969	0.0931969	0.0931904	0.0000065	0.01
10^8	0.2941252	0.2941252	0.2938590	0.0002662	0.09
10^9	NaN	0.9295189	0.9291945	0.0003244	0.03
10^{10}	NaN	2.9388112	2.9089523	0.0298588	1.03
$1.4\cdot10^{10}$	NaN	3.4771987	3.4080757	0.0691230	2.03

TABLE VI
COMPARISON OF THE RESISTANCE PER UNIT LENGTH OF COAXIAL WAVEGUIDE FROM THE SECOND EXAMPLE

f	L Matlab without fictional layers	L Matlab with fictional layers	L ANSYS	ΔL Matlab - ANSYS	ΔL
Hz	μH/m	μH/m	μH/m	μH/m	%
10^0	0.245251	0.245251	0.245295	0.000044	0.018
10^1	0.245251	0.245251	0.245295	0.000044	0.018
10^2	0.245240	0.245240	0.245284	0.000044	0.018
10^3	0.244192	0.244192	0.244236	0.000044	0.018
10^4	0.212730	0.212730	0.212776	0.000045	0.021
10^5	0.181437	0.181437	0.181477	0.000040	0.022
10^6	0.171348	0.171348	0.171387	0.000039	0.023
10^7	0.168151	0.168151	0.168189	0.000038	0.023
10^8	0.167139	0.167139	0.167146	0.000006	>0.01
10^9	NaN	0.166820	0.166826	0.000006	
10^{10}	NaN	0.166719	0.166724	0.000006	
$1.4\cdot10^{10}$	NaN	0.166711	0.166717	0.000005	

The absolute difference between modules of characteristic impedance is between 0.014 Ω and 1 Ω, which corresponds to relative differences of 0.03% and 0.06%, respectively. Numbers presented in Tab. IV, V and VI show strong agreement between results obtained from the our analytical formulas and FEM simulations. There is no significant difference between results obtained with Matlab models with and without "fictional" layers. Table V presents resistance per unit length of a waveguide with and without fictional layers. These results were calculated using Matlab and validated with FEM simulations. The difference between them is from 0.0000006 to 0.0691230 Ω/m, which corresponds to 0.04% and 2.03%, respectively. It confirms correctness of results obtained with the new analytical formula up to 1 GHz. At 1 GHz and above, the relative difference is increasing from 0.03%, through 1.03% up to 2.03% at 14 GHz. The increase in error is caused by the operation of the waveguide near the cut-off frequency. Despite of this, the relative difference is ≤ 2%, which also confirms correctness of the developed model. Again, there is no significant difference between results obtained using Matlab model with and without "fictional" layers.

As the last parameter, inductance per unit length was calculated and presented in Table VI. The relative difference between results is from 0.01% to 0.023% in the assumed frequency range. Like before, there is no significant difference between inductance per unit length computed by the Matlab formula with and without additional fictional layers. Moreover, the upper limit of calculation was extended from 100 MHz to 14 GHz. The capacitance calculated with the new analytical Matlab formula and FEM simulations is equal to 66.83 and 66.77 pF/m, respectively. It corresponds to absolute difference of 0.06 pF/m or relative difference of 0.09%.

IV. CONCLUSION

The new robust and numerically stable algorithm presented in the article can be used for calculation of wave impedance and its components of cylindrical coaxial waveguides composed of unlimited number of layers. The presented analytical formula was checked with FEM ANSYS models in frequency range depending on geometries and dimensions of the waveguide, especially for thin and thick layers. The results of the comparison well agree with results obtained with the new analytical model and FEM simulations. The achieved relative error of the module of characteristic impedance between presented methods, for discussed frequency range, is much lower than 0.1%, which proves the correctness of the new analytical approach.

The presented work shows also that in case of calculations performed for thick layers at higher frequencies it is necessary to divide the thick layer into additional "fictional" layers to provide numerical stability. The results of calculations also assured, that the additional "fictional" layers do not degrade their accuracy. Moreover, results obtained for models with and without additional "fictional" layers are identical. The latter case allows an easy extension of frequency range without sacrificing the numerical stability. The presented algorithm allows much faster computations of characteristic impedance of coaxial waveguides than FEM and does not require a high-performance computer.

The method is especially useful for optimization of cylindrical multilayer waveguides for wideband calculable thermal converters used in voltage AC-DC transfer and precision high frequency current shunts.

REFERENCES

[1] Y. Shan, Y. Meng and P. Filipski, „Evaluation of a Calorimetric Thermal Voltage Converter for RF–DC Difference up to 1 GHz", *IEEE Transactions on Instrumentation and Measurement*, vol. 63, no. 2, pp. 467-472, 2014. https://doi.org/10.1109/TIM.2013.2278597

[2] P. Filipski, C. van Mullem, D. Janik, M. Klonz, J. Kinard, T. Lipe and B. Waltrip, „Comparison of high-frequency AC-DC voltage transfer standards at NRC, VSL, PTB, and NIST", *IEEE Transactions on Instrumentation and Measurement*, vol. 50, no. 2, pp. 349-352, 2001. http://doi.org/10.1109/TIM.2013.2278597

[3] M. Malinowski, K. Kubiczek and M. Kampik, „A precision coaxial current shunt for current AC-DC transfer", *Measurement*, vol. 176, p. 109126, 2021. http://doi.org/10.1016/j.measurement.2021.109126

[4] M. Malinowski et al., „A Precision Coaxial Low-Current Shunt with Improved Mathematical Model", *2021 13th International Conference on Measurement*, 2021.

[5] G. Kyriazis, R. de Souza, E. Yasuda and L. Di Lillo, „Modeling the AC–DC Transfer Difference of Wideband Cage-Type Current Shunts", *IEEE Transactions on Instrumentation and Measurement*, vol. 69, no. 7, pp. 4436-4444, 2020. http://doi.org/10.1109/TIM.2019.2944012

[6] A. Andreychenko, H. Kroeze, D. Klomp, J. Lagendijk, P. Luijten and C. van den Berg, „Coaxial waveguide for travelling wave MRI at ultrahigh fields", *Magnetic Resonance in Medicine*, vol. 70, no. 3, pp. 875-884, 2012. https://doi.org/10.1002/mrm.24496

[7] H. Bao, K. Nielsen, O. Bang and P. Jepsen, „Dielectric tube waveguides with absorptive cladding for broadband, low-dispersion and low loss THz guiding", *Scientific Reports*, vol. 5, no. 1, 2015. https://doi.org/10.1038/srep07620

[8] J. Melzer, M. Navarro-Cía, O. Mitrofanov and J. Harrington, „Silver-coated Teflon hollow waveguides for the delivery of terahertz radiation", *Optical Fibers and Sensors for Medical Diagnostics and Treatment Applications XIV*, 2014.

[9] S. Khalili, M. Botshekanan Dehkordi and E. Carrera, „A nonlinear finite element model using a unified formulation for dynamic analysis of multilayer composite plate embedded with SMA wires", *Composite Structures*, vol. 106, pp. 635-645, 2013. https://doi.org/10.1016/j.compstruct.2013.07.006

[10] Z. Mikno, M. Stepien and B. Grzesik, „Optimization of resistance welding by using electric servo actuator", *Welding in the World*, vol. 61, no. 3, pp. 453-462, 2017. http://doi.org/10.1007/s40194-017-0437-x

[11] M. Stepien, S. Krosny and B. Grzesik, „Analysis of quench propagation using coupled electrical-thermal FEM model", *Journal of Physics: Conference Series*, vol. 234, no. 2, p. 022036, 2010. https://doi.org/10.1088/1742-6596/234/2/022036

[12] G. Aiello, S. Alfonzetti, E. Dilettoso and N. Salerno, „Eddy Current Computation by the FEM-SDBCI Method", *IEEE Transactions on Magnetics*, vol. 52, no. 3, pp. 1-4, 2016. https://doi.org/10.1109/TMAG.2015.2483367

[13] S. Krosny, M. Woźniak, S. Hopkins, M. Stępień, B. Grzesik and B. Glowacki, „Modelling of transient state phenomena of composite superconducting conductors during pulse Ic(B) measurements", *Journal of Physics: Conference Series*, vol. 234, no. 2, p. 022019, 2010. https://doi.org/10.1088/1742-6596/234/2/022019

[14] K. Kubiczek and M. Kampik, „Highly accurate and numerically stable computations of double-layer coaxial waveguides", *Engineering Computations*, 2019. Available: http://doi.org/10.1108/EC-09-2018-0415

[15] C. Paul, *Introduction to electromagnetic compatibility*. Hoboken, N.J.: Wiley, 2006, pp. 871-900.

[16] J. Jackson, *Classical electrodynamics*. New Delhi: Wiley India, 2011, pp. 69-75.

[17] H. W. Dommel, "Overhead line parameters from handbook formulasand computer programs", with discussions by A. Deri and G. Tevan, Adam Semlyen, and F. L. Alvarado, IEEE Trans., Power Appar. Syst., 1985, 104, (2), pp. 366–372

[18] H. W. Dommel, "EMTP Theory Book", Microtran Power System Analysis Corporation, Vancouver, British Columbia:, 1992, 2nd Edn.

[19] S. Vujević, V. Boras, P. Sarajčev, „A novel algorithm for internal impedance computation of solid and tubular cylindrical conductors", *International Review of Electrical Engineering (IREE).* Vol.4, Part B, pp. 1418-1425, 2009.

[20] N. Nahman and D. Holt, „Transient analysis of coaxial cables using the skin effect approximation $A+B\sqrt{s}$ „, *IEEE Transactions on Circuit Theory*, vol. 19, no. 5, pp. 443-451, 1972.

[21] A. Semlyen and A. Deri, „Time Domain Modeling of Frequency Dependent Three-Phase Transmission Line Impedance", *IEEE Power Engineering Review*, vol. -5, no. 6, pp. 64-65, 1985.

[22] S. Vujevic and D. Lovric, „On the numerical computation of cylindrical conductor internal impedance for complex arguments of large magnitude", *Facta universitatis - series: Electronics and Energetics*, vol. 30, no. 1, pp. 81-91, 2017. http://doi.org/10.2298/FUEE1701081V

[23] S. Vujevic, D. Lovric and V. Boras, „High-Accurate Numerical Computation of Internal Impedance of Cylindrical Conductors for Complex Arguments of Arbitrary Magnitude", *IEEE Transactions on Electromagnetic Compatibility*, vol. 56, no. 6, pp. 1431-1438, 2014. http://doi.org/10.1109/temc.2014.2352398

[24] J. Carson and J. Gilbert, „Transmission characteristics of the submarine cable", *Journal of the Franklin Institute*, vol. 192, no. 6, pp. 705-735, 1921.

[25] J. A. Brandao Faria, „A matrix approach for the evaluation of the internal impedance of multilayered cylindrical structures", *Progress In Electromagnetics Research B, Vol. 28, 351-367, 2011.*

[26] K. Kubiczek and M. Kampik, „Highly Accurate and Numerically Stable Matrix Computations of the Internal Impedance of Multilayer Cylindrical Conductors", *IEEE Transactions on Electromagnetic Compatibility*, pp. 1-8, 2019. Available: http://doi.org/10.1109/TEMC.2018.2890447

[27] ANSYS Academic Multiphysics Campus Solution 2017. „Engineering Simulation & 3-D Design Software | ANSYS", Ansys.com, 2019. [Online]. Available: Available: https://www.ansys.com/.

[28] U. Bakshi and A. Bakshi, *Transmission lines and waveguides*. 70p.: Ill., pp. 24, ch.1.

[29] P. Peres, C. de Souza and I. Bonatti, „ABCD Matrix: A Unique Tool for Linear Two-Wire Transmission Line Modelling", *International Journal of Electrical Engineering Education*, vol. 40, no. 3, pp. 220-229, 2003.

[30] S. Schelkunoff, "The Electromagnetic Theory of Coaxial Transmission Lines and Cylindrical Shields", *Bell System Technical Journal*, vol. 13, no. 4, pp. 532-579, 1934.

[31] J. H. Poynting, "On the transfer of energy in the electromagnetic field", *Philosophical Transactions of the Royal Society of London*. 175: 343–361, 1884**.**

[32] D. Lovric and S. Vujevic, „Accurate Computation of Internal Impedance of Two-Layer Cylindrical Conductors for Arguments of Arbitrary Magnitude", *IEEE Transactions on Electromagnetic Compatibility*, vol. 60, no. 2, pp. 347-353, 2018. http://doi.org/10.1109/TEMC.2017.2715985

[33] A. Gil, J. Segura and N. Temme, „Computing solutions of the modified bessel differential equation for imaginary orders and positive arguments", *ACM Transactions on Mathematical Software*, vol. 30, no. 2, pp. 145-158, 2004. http://doi.org/10.1145/992200.992203

[34] N. Marcuvitz, *Waveguide handbook*. New York: McGraw-Hill, 1951, pp. 72-80.